

ORIGINAL RESEARCH ARTICLE

Carbon turnover and microbial activity in an artificial soil under imposed cyclic drainage and imbibition

Geertje J. Pronk^{1,2*} | Adrian Mella^{2,3*} | Tatjana Milojevic^{2,4} |
Christina M. Smeaton^{2,5} | Katja Engel⁶ | Josh D. Neufeld⁶ | Fereidoun Rezanezhad² |
Philippe Van Cappellen²

¹KWR Water Cycle Research Institute, Groningenhaven 7, Nieuwegein, 3433 PE, the Netherlands

²Water Institute and Dep. of Earth & Environmental Sciences, Univ. of Waterloo, 200 University Ave. W., Waterloo, ON, N2L 3G1, Canada

³Center for Applied Geoscience, Hydrogeology, Univ. of Tübingen, Hölderlinstraße 12, Tübingen, 72074, Germany

⁴Lab. of Cryospheric Sciences, School of Architecture, Civil and Environmental Engineering, École polytechnique fédérale de Lausanne, Lausanne, Switzerland

⁵School of Science and the Environment, Grenfell Campus, Memorial Univ. of Newfoundland, 20 University Dr., Corner Brook, NL, A2H 5G4, Canada

⁶Dep. of Biology, Univ. of Waterloo, 200 University Ave. W., Waterloo, ON, N2L 3G1, Canada

Correspondence

Adrian Mella, Center for Applied Geoscience, Hydrogeology, Univ. of Tübingen, Hölderlinstraße 12, Tübingen, 72074, Germany.

Email: adrian.mella@uni-tuebingen.de

Funding information

Canada Excellence Research Chair (CERC) Program; Deutsche Forschungsgemeinschaft, Grant/Award Number: PR1550/1-1

*Geertje J. Pronk and Adrian Mella contributed equally to this work.

Abstract

Water table fluctuations generate temporally and spatially dynamic physicochemical conditions that drive biogeochemical hot spots and hot moments in the vadose zone. However, their role in the cycling of soil C remains poorly known. Here, we present results from unvegetated column experiments filled with 45 cm of artificial soil containing 10% humus, and inoculated with a natural microbial extract. In one series of three replicate columns, five cycles, each consisting of a 4-wk drainage followed by a 4-wk imbibition period, were imposed, whereas in a second series, the water table remained static. Depth-resolved O₂ concentration profiles and headspace CO₂ effluxes were markedly different between the two regimes. In the fluctuating regime, drainage periods yielded 2.5 times greater CO₂ effluxes than imbibition periods. At the end of the experiment, the fluctuating water table columns exhibited a distinct zone of organic C (OC) depletion in the depth interval of 8–20 cm that was not observed under the static regime. Although this zone showed elevated levels of adenosine triphosphate (ATP), the microbial biomass was actually lower than at the corresponding depth interval of the static regime. A vertically stratified microbial community established in all columns that depended on oxygenation with depth. The 16S ribosomal RNA (rRNA) gene analyses showed a slightly higher diversity in the

Abbreviations: ATP, adenosine triphosphate; bss, below the soil surface; DIC, dissolved inorganic carbon; DOC, dissolved organic carbon; MBC, microbial biomass carbon; OC, organic carbon; OTU, operational taxonomic unit; rRNA, ribosomal RNA.

This is an open access article under the terms of the Creative Commons Attribution License, which permits use, distribution and reproduction in any medium, provided the original work is properly cited.

© 2020 The Authors. *Vadose Zone Journal* published by Wiley Periodicals, Inc. on behalf of Soil Science Society of America

soil exposed to moisture fluctuations, but there was no clear difference in major taxa and microbial community composition between treatments. These results thus suggest that the localized enhancement of OC degradation induced by the water table fluctuations was driven by a more active, rather than a more abundant or compositionally very different, microbial community.

1 | INTRODUCTION

The vadose zone is characterized by steep spatially and temporally varying physical and chemical gradients (Haberer, Rolle, Cirpka, & Grathwohl, 2012; Jost, Winter, & Gallert, 2011), which enhance biogeochemical activity and promote microbial diversity (Berkowitz, Silliman, & Dunn, 2004; Rezanezhad, Couture, Kovac, O'Connell, & Van Cappellen, 2014). The vadose zone, and in particular the capillary fringe, are therefore considered to be biogeochemical "hot spots" (McClain et al., 2003). Previous studies have further shown that water table oscillations act as a major forcing on soil biogeochemistry that may accelerate the degradation of organic matter and influence the release of CO₂, CH₄, and N₂O (Hefting et al., 2004; Klüpfel, Piepenbrock, Kappler, & Sander, 2014; Pett-Ridge, Silver, & Firestone, 2006; Yu, Faulkner, & Baldwin, 2008).

Soil moisture is a primary factor controlling the delivery of O₂ along the soil profile, which is in turn linked to the availability and utilization of other electron acceptors and, consequently, to the rate and mechanisms of soil organic C (OC) degradation (Keiluweit, Nico, Kleber, & Fendorf, 2016; Moyano, Manzoni, & Chenu, 2013). Therefore, understanding how subsurface soil biogeochemical functioning responds to periodic variations in oxygenation mediated by groundwater table fluctuations is essential for predicting the fate and turnover of soil organic matter and the associated soil-atmosphere gas exchanges (Klüpfel et al., 2014; Moyano et al., 2013).

In a fluctuating water table riparian-soil column experiment, Rezanezhad et al. (2014) found that transient redox conditions enhanced microbial oxidation of soil OC, and that water table drawdown yielded peak CO₂ emissions. Moisture content and redox conditions influence both microbial activity and the development of microbial communities in soils by inducing water potential stress and modulating the delivery of energy yielding electron acceptors (Jost et al., 2011). Pore-network connectivity also affects the interactions within bacterial communities because of different abilities to use electron acceptors and metabolize substrates under varying redox potentials (Dassonville & Renault, 2002; Vos, Wolf, Jennings, & Kowalchuk, 2013). Pett-Ridge et al. (2006) and DeAngelis, Silver, Thompson, and Firestone (2010) assessed the effects of

redox conditions on the microbial community composition of a humid tropical soil by carrying out incubation experiments under oxic, anoxic, and fluctuating (oxic–anoxic) redox conditions. Their results showed that the microbial biomass concentration and community composition remained stable under redox fluctuating conditions. However, the biomass concentrations decreased and the microbial composition changed under both the static oxic and static anoxic conditions. These findings thus imply that frequent depletion and resupply of O₂ may enhance microbial tolerance to changing environmental conditions.

Soil incubation experiments are often carried out with natural soils. The latter are inherently complex matrices, making it often difficult to identify all the factors and interactions controlling soil C cycling. The use of model matrices, such as artificial soil mixtures, provides an alternative approach for answering specific research questions. With an artificial soil, the initial conditions, including the composition and structure of the soil matrix, are well defined and artifacts related to heterogeneity are minimized (Pronk et al., 2017). Previous experiments with artificial soils have helped elucidate the specific roles of mineral components in soil development, the formation of organo–mineral associations, and microbial community changes (Ding et al., 2013; Pronk, Heister, Ding, Smalla, & Kögel-Knabner, 2012).

Here, we present results from soil column incubations in which columns packed with a well characterized artificial soil as starting material were subjected to cycles of drainage and imbibition, whereas in identical control columns, the water table was held at a fixed position. The soil columns were spiked with a microbial inoculum isolated from a natural soil environment. The responses to the imposed hydraulic regimes were monitored by measuring greenhouse gas effluxes, depth-dependent redox potentials, and dissolved O₂ concentrations, and by periodically sampling and analyzing the pore-water chemistry. At the end of the incubations (329 d), the cores were sliced and the depth distributions of OC, microbial biomass, adenosine triphosphate (ATP) concentrations, and the microbial community composition were determined. The results shed new light on the response of the microbial community to dynamic oxygenation and moisture conditions, as well as the consequences for OC turnover.

2 | MATERIALS AND METHODS

2.1 | Artificial soil columns

Six clear hard acrylic columns, with 7.5-cm i.d. and 60-cm length, were each packed with 45 cm of a homogeneous artificial soil mixture at an initial average bulk density of 1 g cm^{-3} , leaving a headspace of $\sim 660 \text{ cm}^3$. Similar to a previously described method (Pronk et al., 2012), the artificial soil was prepared by dry mixing 77.5% quartz sand (3Q-ROK, US Silica), 10% montmorillonite (Ceratossil WG, Süd Chemie), 2.5% goethite (Bayoxide EF 200, Lanxess), and 10% organic matter collected from the H-horizon humus of a mixed deciduous forest soil at the *rare* Charitable Research Reserve, Cambridge, ON, Canada. The organic matter was air dried, homogenized, sieved ($< 2 \text{ mm}$), and used without sterilization. Dibasic calcium phosphate (0.8 mg g^{-1}) was added as a P supplement. After mixing, the soil was partially wetted with synthetic groundwater and inoculated with the water extractable microbial community extracted from the same humus at a ratio of $6 \text{ g humus kg}^{-1}$ soil (Pronk et al., 2012). Synthetic deoxygenated groundwater was prepared to match the major ion chemistry of the local groundwater at the *rare* site where the organic matter was collected: KHCO_3 (0.5 mM), CaCl_2 (1 mM), and MgCl_2 (1 mM). The OC content measured on the initial artificial soil mixture was $35 \pm 3 \text{ mg g}^{-1}$, the molar C/N ratio was 36, and the soil water pH was 7.5.

2.2 | Incubation regimes

Two sets of triplicate columns were incubated under two contrasting treatments: static and fluctuating. The columns are hereafter referred to as C1, C2, and C3 for the static (control) columns and F1, F2, and F3 for the fluctuating columns. The hydraulic regimes were imposed as shown in Figure 1 and described in detail in Rezanezhad et al. (2014). Briefly, a programmable multichannel pump regulated the water level in a hydrostatic equilibrium reservoir by flowing water in (out) from (to) a water storage reservoir. A hydrostatic equilibrium reservoir was hydraulically connected to the three replicate soil columns in each of the two hydraulic treatments. Raising or lowering the water level in the hydrostatic equilibrium column then caused the water level in the soil columns to either rise or drain.

The water table in the static columns was held at a depth of 20 cm below the soil surface (bss) for the entire duration of the experiment. Some water was added to the equilibrium column on a weekly basis to compensate for evaporative loss. In the fluctuating water table treatment, five consecutive drainage and imbibition cycles were imposed. Imbibition was imposed by instantaneously increasing the water level in the equilibrium column to the height of the soil surface

Core Ideas

- Artificial soil columns were incubated with natural soil microbial inoculum.
- Replicates were subjected to cycles of drainage and imbibition.
- Drainage after water-logged conditions led to pronounced pulses of CO_2 efflux.
- Incubation treatment yielded distinct zone of OC depletion in the fluctuation zone.
- Enhanced turnover was driven by more active and not more diverse biomass community.

(0 cm) and maintaining that level for 28 d. Thus, water flowed into the soil-packed columns from the equilibrium reservoir (Figure 1). During drainage, the water level was lowered from 0 to 40 cm bss by allowing free drainage of the soil columns into an outflow reservoir. The drainage volume was measured and samples were collected for chemical analysis. When the water level in the equilibrium reservoir reached 40 cm bss, it was held there for 28 d until the next cycle.

The columns were incubated in the dark at $23.6 \pm 1.6 \text{ }^\circ\text{C}$. The headspace of the soil columns was flushed with water-saturated air through the upper ports of the columns to minimize evaporative loss, whereas the hydrostatic equilibrium reservoirs were sparged continuously with Ar gas to ensure anoxic conditions. Columns C1 and F1 were sacrificed 99 d after the start of incubation, after the completion of the first drainage and imbibition cycle. Columns C2, C3, F2, and F3 were incubated for 329 d before being sampled sacrificially.

2.3 | In situ sensors and pore water sampling

The columns were provided with regularly spaced ports for installing redox potential (E_h) and O_2 sensors and extracting pore water along the depth profile of the columns (Figure 1). Pore water samples were periodically collected with ceramic MicroRhizon samplers (5-cm length, 2.5-mm diam., with a filter pore size of $0.15 \text{ }\mu\text{m}$; CSS5 MicroRhizon, #19.21.23F). The ceramic samplers were installed at 5-, 15-, 25-, and 35-cm depth bss in all soil columns. Up to 5 ml of pore water was extracted every 2 to 4 wk using a vacuum pump set at -100 mbar . However, in the static water table columns, little or no pore water could be extracted at depths above the water table.

High-resolution E_h measurements were carried out at 5-min intervals with glass-tip microelectrodes that were combined with an open-ended gel-stabilized reference electrode that was in contact with the bottom inflow and outflow of the

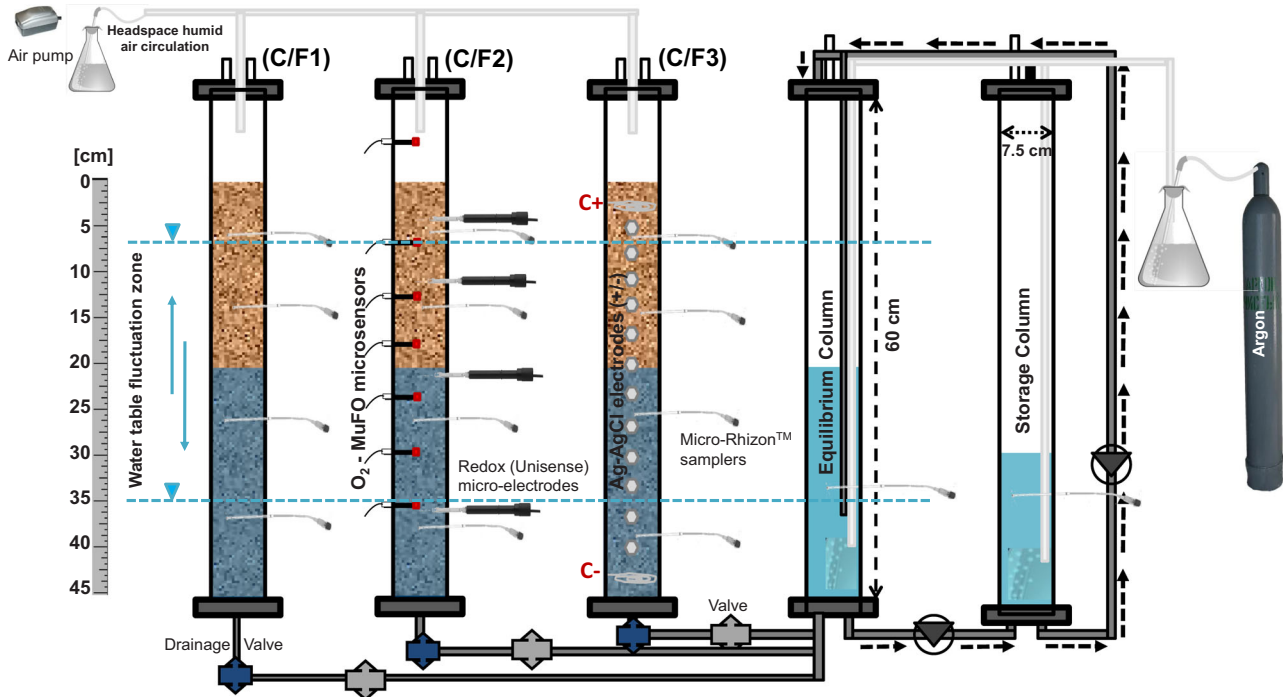


FIGURE 1 Triplicate soil column experimental setup adapted from Rezanezhad et al. (2014). Each water table treatment, static (C) and fluctuating (F), comprises three replicates. All replicate soil-packed columns are hydraulically connected to an equilibrium water reservoir (equilibrium column) that controls the pressure head at the lower boundary of the soil columns and enables the transitions from drainage (drop in equilibrium reservoir level) to imbibition (rise in reservoir level) and vice versa

soil column (10 μm tip diameter, Unisense). The E_h electrodes were installed in column C1 at depths of 3 and 37 cm bss, and in column F2 at depths of 3, 10, 21, and 37 cm bss. Dissolved O_2 was measured every 3 h using an in-house developed luminescence-based optode sensor consisting of fiber optic cables with Pt(II) meso-tetra(pentafluorophenyl)porphine (PtTFPP) sensing and imaging tips (Badocco, Mondin, & Pastore, 2012). The sensing tips were inserted at 2.5, 8.5, 14.5, 20.5, 26.5, and 32.5 cm bss in columns C2 and F2. The uncoated imaging ends were placed in front of a digital single-lens reflex (DSLR) camera with blue light-emitting diode (LED) light of 447.5-nm wavelength (Larsen, Borisov, Grunwald, Klimant, & Glud, 2011). The LED illumination provided an excitation light source to trigger the emission of PtTFPP luminescence. The emitted light was photographed and the light intensity was analyzed using ImageJ software (Rasband, 2015). The Stern–Volmer (SV) equation relates the intensity to the O_2 concentration:

$$\frac{I_0}{I} = 1 + K'_{sv} [\text{O}_2] \quad (1)$$

where I_0 denotes the emitted light intensity in the absence of O_2 , I is the light intensity in the presence of O_2 , $[\text{O}_2]$ is the concentration of O_2 , and K'_{sv} is the SV constant (Badocco et al., 2012).

Columns C3 and F3 were also fitted with nonpolarizing Ag–AgCl potential electrodes and Ag–AgCl current coil electrodes for spectral induced polarization (SIP) and electrochemical potential (EP) measurements (Figure 1). The acquisition of the geoelectrical signals is part of a separate study. Because the SIP and EP records are not essential to the interpretations of the biogeochemical and microbiological data, they are not presented here.

2.4 | Aqueous analyses

The extracted pore water and drainage water samples were subsampled for analysis of dissolved OC (DOC), SO_4^{2-} , Fe^{2+} , electrical conductivity (EC), and pH. The DOC measurements were performed on samples acidified by adding 20 μl of 1 M HCl into 1 ml of sample, then analyzed via the nonpurgeable OC method on a total C analyzer (Shimadzu TOC-LCPH/CPN, method detection limit = 0.011 mM). For analysis of Fe^{2+} with the ferrozine method of Viollier, Inglett, Hunter, Roychoudhury, and Van Cappellen (2000), subsamples were immediately placed in an anaerobic chamber (Coy, $<0.0014 \text{ mg L}^{-1} \text{ O}_2$ in N_2 with 3% H_2). Analysis of SO_4^{2-} was done by ion chromatography (Dionex ICS-5000; method detection limit = 0.27 μM). Both pH and EC were measured using a handheld probe (Horiba B-213

LAQUATwin pH/EC). Because unsaturated conditions and filter membrane clogging occasionally impeded extraction of the full pore water volume, not all the analyses could be performed at all sampling times. This was particularly true for the upper parts of the columns above 20 cm bss.

2.5 | Headspace gas fluxes

The headspace of columns C1, C2, F1, and F2 was sampled every 1–2 d by connecting the two lateral headspace ports to an automated multiplexer CO₂ flux measurement system (Figure 1; LI-8100, LI-COR Biosciences). The measurement setup and procedure are outlined elsewhere (Rezanezhad et al., 2014). Briefly, the CO₂ efflux rate was obtained from the rate of concentration increase within the headspace ($d\text{CO}_2/dt$, $\mu\text{mol m}^{-2} \text{s}^{-1}$), following the method of Davidson, Savage, Verchot, and Navarro (2002). Effluxes of CH₄ and N₂O were determined weekly. Samples were collected at 0 and 30 min after sealing the headspace. Gas analyses were carried out on a gas chromatograph (Model GC-2014, Shimadzu) equipped with an electron capture detector (ECD) and flame ionization detector (FID). The detection limit was 0.28 $\mu\text{g L}^{-1}$ for CH₄ and 0.04 $\mu\text{g L}^{-1}$ for N₂O.

2.6 | Soil analyses

Solid-phase analyses were performed on soil material retrieved from columns C1 and F1 after 99 d of incubation, and for the other columns at the end of the incubation (329 d). The soil was extruded from the columns using a lifting jack and sliced every 2 cm as described in Rezanezhad et al. (2014). Prior to homogenizing a soil slice, it was subsampled for gravimetric determination of bulk density (ρ_b) and water content determination by oven drying of a known volume at 105 °C for 24 h. The remaining material was then homogenized and subsampled for microbial biomass C (MBC) and ATP measurements, as well as DNA sequencing. Additional 10-g subsamples were frozen at –20 °C, freeze dried, ground to fine powder, and analyzed for total OC, inorganic C, and N concentrations using a CHNS Carbo Erba analyzer (method detection limit = 0.1% dry).

The concentrations of ATP were determined in all columns at eight specified depths. For extraction and analysis, ~2 g of soil were flash frozen in liquid N₂ and stored at –20 °C. The methods of Jenkinson and Oades (1979) and Redmile-Gordon, White, and Brookes (2011) were used for extracting ATP from the soil samples. In our adaptation of the methods, HEPES buffer [4-(2-hydroxyethyl)-1-piperazineethanesulfonic acid] replaced the arsenate buffer; we found that 20 mM HEPES adequately buffered the samples to pH 7 without interfering with the luminescence

measurements. Briefly, duplicate samples were extracted by adding TIP reagent (Redmile-Gordon et al., 2011; TIP = 0.92 M trichloroacetic acid, 0.59 M imidazole, and 0.47 M Na₂HPO₄) at a solid/liquid ratio of 0.1 ml TIP g⁻¹ soil, then sonicated for 2 min, placed on ice for 8 min, and filtered (Whatman 42, 2.5- μm pore size). The extract was flash frozen and stored at –20 °C until analysis. Concentrations of ATP were determined through triplicate luminescence measurements on a FlexStation 3 multi-mode microplate reader (Molecular Devices) in multiwell-plate format using a cell viability assay kit (BacTiter-Glo microbial cell viability assay). Following Apostol, Miller, Ratto, and Kelner (2009), limits of quantification and detection of 0.03 and 0.01 nmol g⁻¹, respectively, were determined from the standard deviations obtained on extracted samples of autoclaved artificial soil.

The chloroform fumigation method was used to extract MBC from soil subsamples (Vance, Brookes, & Jenkinson, 1987). Approximately 2 g of soil was extracted with 0.5 M K₂SO₄, either after 24-h exposure to chloroform or without fumigation. The DOC concentration of the extracts (both fumigated and nonfumigated sample extracts) were analyzed, and the extractable MBC concentrations were calculated from the difference between the DOC concentrations in the fumigated and nonfumigated samples. Note that the determination of MBC was only performed on the columns sampled at the end of the incubations.

2.7 | Microbial community composition

A 2-g soil subsample from each soil depth interval (i.e., slice) was immediately frozen in liquid N and stored at –20 °C for 16S ribosomal RNA (16S rRNA) gene analysis. Total DNA was extracted from randomized samples (0.25–0.40 g) using the PowerSoil HTP 96 kit (MO BIO Laboratories). After addition of bead solution (750 μl) and Solution C1 (60 μl), the bead plate was incubated at 70 °C for 10 min before beadbeating at 30 Hz for 2 \times 10 min on a MM 400 mixer mill (Retsch). Genomic DNA was quantified using the Qubit dsDNA HS assay kit (Invitrogen), and fluorescence was measured on a FilterMax F5 Multimode plate reader (Molecular Devices) at 485/525 nm of excitation/emission.

The 16S rRNA genes were amplified using universal prokaryotic primers Pro341F and Pro805R (Joergensen & Mueller, 1996; Takahashi, Tomiata, Nishioka, Hisada, & Nishijima, 2014), containing a unique six base index sequence for sample multiplexing, as well as Illumina flow cell binding and sequencing sites (Bartram, Lynch, Stearns, Moreno-Hagelsieb, & Neufeld, 2011). The 25 μl polymerase chain reaction (PCR) mix contained 1 \times ThermoPol buffer, 0.2 μM forward primer, 0.2 μM reverse primer, 200 μM deoxynucleotides (dNTPs), 15 μg bovine serum albumin, 0.625 U Hot

Start Taq DNA polymerase (New England Biolabs), and 1–20 ng template. Each PCR was prepared in triplicate using an epMotion 5075 liquid handling robot (Eppendorf). The PCR was performed as follows: 95 °C for 3 min, 35 cycles of 95 °C for 30 s, 55 °C for 30 s, 68 °C for 1 min, and a final extension of 68 °C for 7 min. Equal quantities of indexed 16S rRNA gene amplicons were pooled, excised from an agarose gel, and purified using Wizard SV gel and PCR clean-up system (Promega). A 5 pM library containing 5% PhiX (Illumina) was sequenced on a MiSeq instrument (Illumina) using a 2 × 250-cycle MiSeq reagent kit version 2 (Illumina).

Paired-end reads were assembled using the paired-end assembler for Illumina sequences (PANDAseq version 2.8; Masella, Bartram, Truszkowski, Brown, and Neufeld, 2012) using a quality threshold of 0.9 and minimum overlap of eight bases. Assembled reads were analyzed using Quantitative Insights Into Microbial Ecology (QIIME version 1.9.0; Caporaso et al., 2010), managed by automated exploration of microbial diversity (AXIOME version 1.5; Lynch, Masella, Hall, Bartram, and Neufeld, 2013). Sequences were clustered into operational taxonomic units (OTUs) with UPARSE (Edgar, 2013) at 97% identity and aligned with the Python Nearest Alignment Space Termination tool (PyNAST version 1.2.2; Caporaso et al., 2010). Representative sequences were classified using the Ribosomal Database Project (RDP version 2.2; Wang, Garrity, Tiedje, and Cole, 2007) with a confidence threshold of 0.8 against the Greengenes database (McDonald et al., 2012). The AXIOME software generated principal coordinate analysis (PCoA) (Gower, 1966) ordinations using Bray–Curtis dissimilarities (Bray & Curtis, 1957). Permutational multivariate analysis of variance (PERMANOVA) (Anderson, 2001) was used for statistical testing of group similarities. The PERMANOVA was conducted with the *adonis* function in the *vegan* package (version 2.4-4) in R (version 3.4.0) with 5,000 permutations. Indicator species analysis (Dufrière & Legendre, 1997) was conducted using a stringent indicator value threshold of 0.9, sequence abundance threshold of 300, and a *p* value cutoff of <.001.

3 | RESULTS AND DISCUSSION

In what follows, we discuss the results obtained on the columns that underwent the drainage–imbibition cycles and compare them with the results under static water table conditions. The full set of results for the fluctuating and static water table columns can be found in the Supporting Information. The discussion further focuses on the data collected between 100 and 329 d. Visual inspection of the pore water O₂ concentration and redox potential data series under fluctuating water table indicated that the soil biogeochemical system required at least 10 wk to relax from its initial conditions. We therefore assumed that beyond 100 d, the observed differences

between the dynamic and static water table soil columns primarily reflected the differences in the hydraulic regimes.

3.1 | Pore water geochemistry

The time series O₂ concentrations measured at five different depths for the fluctuating water table are presented in Figure 2, along with pore water pH and DOC measurements and headspace CO₂ fluxes. Note that the figure shows the pore water pH and DOC data for both columns F2 and F3, but only the O₂ concentrations and CO₂ fluxes measured in column F2. The complete time-series pore water geochemical data for DOC, SO₄²⁻, and Fe²⁺, for both dynamic and static water table regimes, are presented in the Supporting Information (Supplemental Figures S1, S2, and S3).

Pore water pH measured at 15 cm bss in both dynamic water table columns F2 and F3 exceeded pH 8 and showed a slight upward trend after 200 d (Figure 2b). The concentrations of DOC clearly recorded the drainage and imbibition periods with variations of up to 8 mM (Figure 2c). During drainage, the DOC concentrations fell, whereas they increased during imbibition. The DOC data also showed good reproducibility between the duplicate columns F2 and F3. Emissions of N₂O were below detection, and those of CH₄ were low, mostly falling between 0.01 and 0.4 μmol m⁻² s⁻¹ (see Supplemental Section S4).

3.2 | Oxygen and redox dynamics

During the three complete drainage and imbibition cycles after Day 100, systematic and consistent variations in the O₂ concentrations were observed in column F2 (Figure 2a). Drainage periods resulted in sharp increases in the O₂ concentrations at depths of 8.5, 14.5, and 20.5 cm bss. At 8.5 and 14.5 cm, the O₂ concentration increases coincided closely with the onset of drainage. The O₂ concentrations asymptotically approached their maximum value (~0.22 mM) within 3–4 d and then remained constant for the remainder of the drainage period. At 20.5 cm, the initial rapid increase of the O₂ concentration was delayed by ~3 d relative to the shallower depths, then slowly rose from 0.12 to 0.20 mM throughout the drainage period. Imbibition periods resulted in a staggered drop in the O₂ concentrations, beginning ~4 d after the start of imbibition at 20.5 cm bss and up to 19 d at 8.5-cm depth.

The observed hysteresis in the response of the O₂ concentrations to drainage and imbibition (i.e., a more lagged response after drainage, with changes occurring well into the imbibition period) likely reflects the hysteresis in the moisture response due to the shrinking and swelling of the 10% montmorillonite in the artificial soil (Saiyouri, Hicher, &

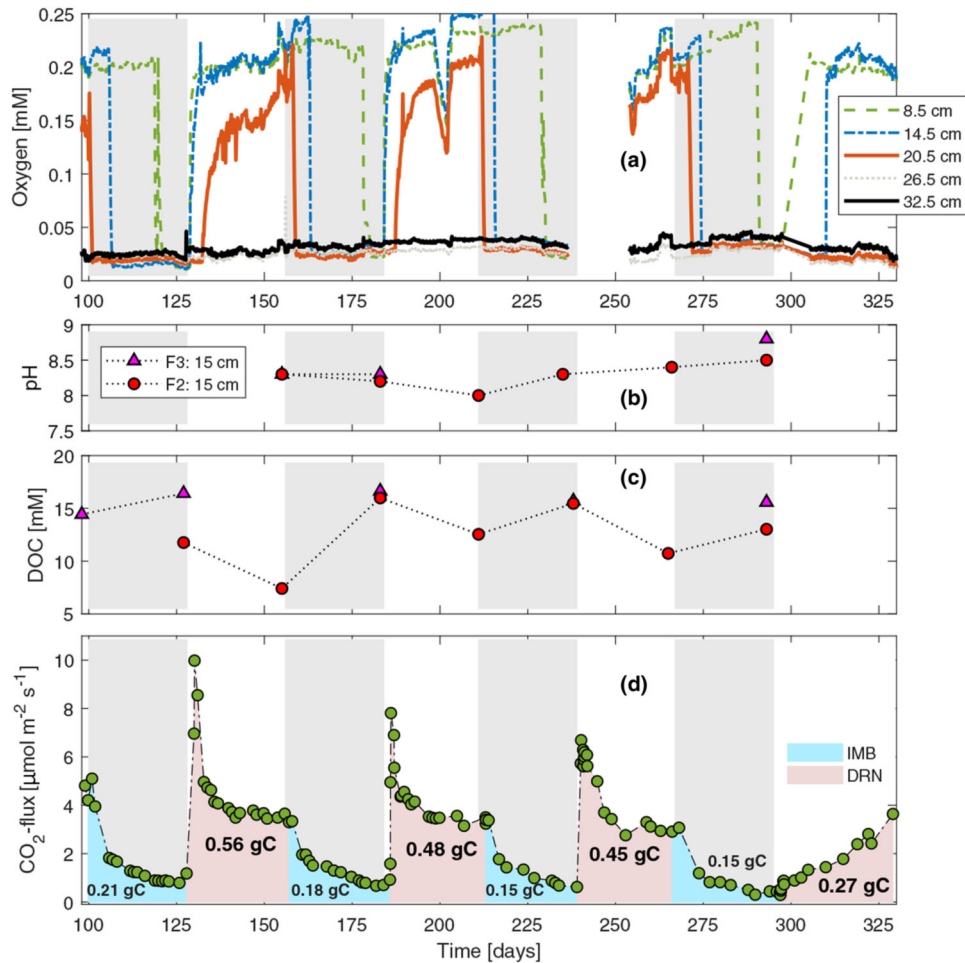


FIGURE 2 Timeseries results for (a) O_2 along the soil depth profile, (b) pore water pH, (c) pore water dissolved organic C (DOC), and (d) headspace CO_2 efflux, measured in the fluctuating treatment, column F2. Optodes for O_2 measurement were only installed in column F2. Alternating gray and white rectangles signify periods of imbibition and drainage, respectively. Porewater data (pH and DOC) are shown for the fluctuation zone (at 15 cm), that is, the depth interval that experienced the most pronounced variations in O_2 . (d) Integrated CO_2 emission (g C) calculated by integrating the CO_2 flux curves over each period—imbibition (IMB, blue) and drainage (DRN, pink)—is plotted under the flux curve, from Day 100 to the end of the experiment

Tessier, 2000; Xie, Agus, Schanz, & Kolditz, 2004). In fact, because of the high water retention capacity, the uppermost soil still retained $\sim 30\%$ water saturation at the end of the 4-wk drainage periods (data not shown). At depths of 26.5 and 32.5 cm bss, the O_2 concentrations were below 0.05 mM with no visible imprint of the fluctuating water table. In the static water table column C2, the O_2 levels showed little temporal variability (Supplemental Figure S4a); the concentrations hovered around 0.25 mM at 8.5 and 14.5 cm bss, then dropped to <0.075 mM at 20 cm and deeper.

The redox potential (E_h) exhibited trends consistent with those of O_2 (Supplemental Figure S5a). The E_h data series, however, was incomplete due to the limited electrode lifetime of around 6 mo. Therefore, largely based on the measured O_2 dynamics under fluctuating water table, we define three depth zones in the fluctuating water table columns to facilitate the presentation and discussion of the results. The *oxic*

zone (0–8 cm) is characterized by the presence of O_2 levels in excess of 0.2 mM during at least two-thirds of the time under the dynamic water table regime. By contrast, the *anoxic zone* (below 20 cm) continuously experienced O_2 levels below 0.05 mM. The *fluctuation zone* (8–20 cm) is the depth interval between the oxic and anoxic zones.

3.3 | Carbon dioxide emissions

Under the dynamic water table regime, a pronounced pulse of CO_2 was emitted shortly after the onset of each drainage period (Figure 2d). Similar CO_2 pulses have been observed in previous soil incubation experiments (Ebrahimi & Or, 2018; Rezanezhad et al., 2014; Wang, Bogena, Vereecken, & Bruggemann, 2018). After the pulse release, the CO_2 flux dropped to a near-constant level during the final 2–3 wk of

the drained period. Both the maximum and final CO₂ flux values decreased with each successive drainage period. The onset of an imbibition period was accompanied by an initial drop in CO₂ flux, followed by a more gradual decline to final values significantly below those observed during the drainage periods.

Compared with the results for column F2, the CO₂ fluxes measured in the static water table column C2 exhibited a slow, monotonic decrease over the 100–329 days of incubation, with values intermediate between those of the drainage and imbibition periods under the fluctuating water table regime (Supplemental Figure S4b). With the exception of the initial CO₂ pulses, the magnitudes of the CO₂ fluxes measured in the fluctuating and stable water table columns fell within the typical range of measurements reported for temperate forest soils over the growing season (1–6 μmol CO₂ m⁻² s⁻¹, e.g.; Epron, Farque, Lucot, & Badot, 1999; Hanson, Wullschleger, Bohlman, & Todd, 1993; Wang et al., 2013). However, the artificial soils were incubated at 23.6 ± 1.6 °C, on average, 5–10 °C warmer than shallow soils during a temperate growing season. Thus, a lower incubation temperature would have resulted in fluxes likely close to the lower limit of the reported range.

Drainage-enhanced CO₂ fluxes are expected because of the concomitant influx of O₂, which stimulates aerobic respiration, in part coupled to the oxidation of soluble fermentation compounds produced under the anoxic conditions of the preceding period of imbibition (Huang et al., 2019; Stegen et al., 2016). The production of fermentation compounds is in line with the observed increase in DOC concentration, at 15 cm, during each imbibition period (see Supplemental Figure S1), which is expected to stimulate CO₂ production (Cleveland, Wieder, Reed, & Townsend, 2010). Our interpretation is consistent with the observed variations in DOC at 15-cm depth in column F2, which suggest consumption of dissolved organic substrates during drainage that were accumulated in the previous imbibition period (Figure 2c). Prolonged anaerobic conditions may also have led to the release of mineral-protected C after Fe reduction (Huang & Hall, 2017). Fluctuations in pore water Fe²⁺ concentrations (see Supplemental Figure S3) provide evidence that Fe reduction took place in the columns, at least during some imbibition periods. Furthermore, the initial CO₂ pulse at the start of the drainage periods may additionally reflect the rapid degassing of previously produced CO₂ to the air-filled pore space created by the lowering of the water table (Oertel, Matschullat, Zurba, Zimmermann, & Erasmi, 2016; Wang et al., 2018). In contrast, decreased CO₂ production during imbibition arises from kinetically and/or thermodynamically constrained C decomposition during O₂ limitation (Keiluweit et al., 2016). Additionally, during the water-logged conditions of the imbibition periods, emission of anaerobically produced CO₂ would be limited by slow diffusion through the pore water network.

The CO₂ emissions integrated over the drainage periods were, on average, 2.5 times higher than those of the imbibition periods (Figure 2). Furthermore, the integrated CO₂ efflux of 0.56 g C during the first drainage period decreased to 0.27 g C for the last drainage period. The integrated CO₂ emissions during the imbibition periods also decreased, albeit more gradually, from 0.21 to 0.15 g C. Vogel et al. (2014) similarly observed gradually declining CO₂ effluxes in soil incubations lasting 562 d. These authors also showed that the CO₂ production could be reactivated by adding fresh organic substrates. The decreasing temporal trends in CO₂ emissions in both fluctuating and static water table columns are therefore ascribed to the progressive depletion of the finite pool of degradable soil organic matter. Contrary to natural soil systems, there is no resupply of new organic substrates in the column experiments, thus causing CO₂ production to slow down with time (Pronk et al., 2017).

3.4 | Organic carbon turnover

The distributions of OC, MBC, and ATP measured at the end of the incubation period (329 d) are presented for both the fluctuating and static water table regimes in Figure 3. The total integrated OC losses in the columns were calculated by subtracting the final OC concentrations from the initial OC content of the artificial soil (35 ± 3 mg g⁻¹). Because of the fairly high OC content of the initial soil, the OC losses were relatively small. Nonetheless, the estimated OC loss relative to the total initial C stock in the fluctuating water table column (8.7 ± 0.9%) was higher than in the static water table column (7.7 ± 0.9%). Most of the difference in OC loss between the two water table regimes was localized within the 8- to 20-cm depth interval—that is, the fluctuation zone defined in Section 3.2 (Figure 3a). A similar mid-column zone of OC depletion under a fluctuating water table has been observed in a previous soil column incubation experiment (Rezanezhad et al., 2014). In this earlier study, the localized depletion of OC was ascribed to enhanced degradation of soil organic matter under the alternating oxic–anoxic conditions driven by the imposed dynamic hydraulic regime.

The total OC loss in the fluctuating water table columns F2 and F3, integrated over the entire duration of the experiment (1–329 d), was estimated from the difference between the OC distributions measured at the end and the initial OC concentration of the homogeneous soil mixture. The resulting OC loss was 5.4 ± 0.7 g C. For comparison, the integrated CO₂ efflux over the 329 d of incubation amounted to 3.9 ± 0.4 g C, or 72% of the OC loss. Note that the reported ± error of integrated CO₂ production was computed based on a 10% overestimation of closed-chamber methods, after Rayment (2000). Figure 3b compares overall OC loss to integrated outflow drainage and gas efflux. Drainage DOC and dissolved inorganic C (DIC)

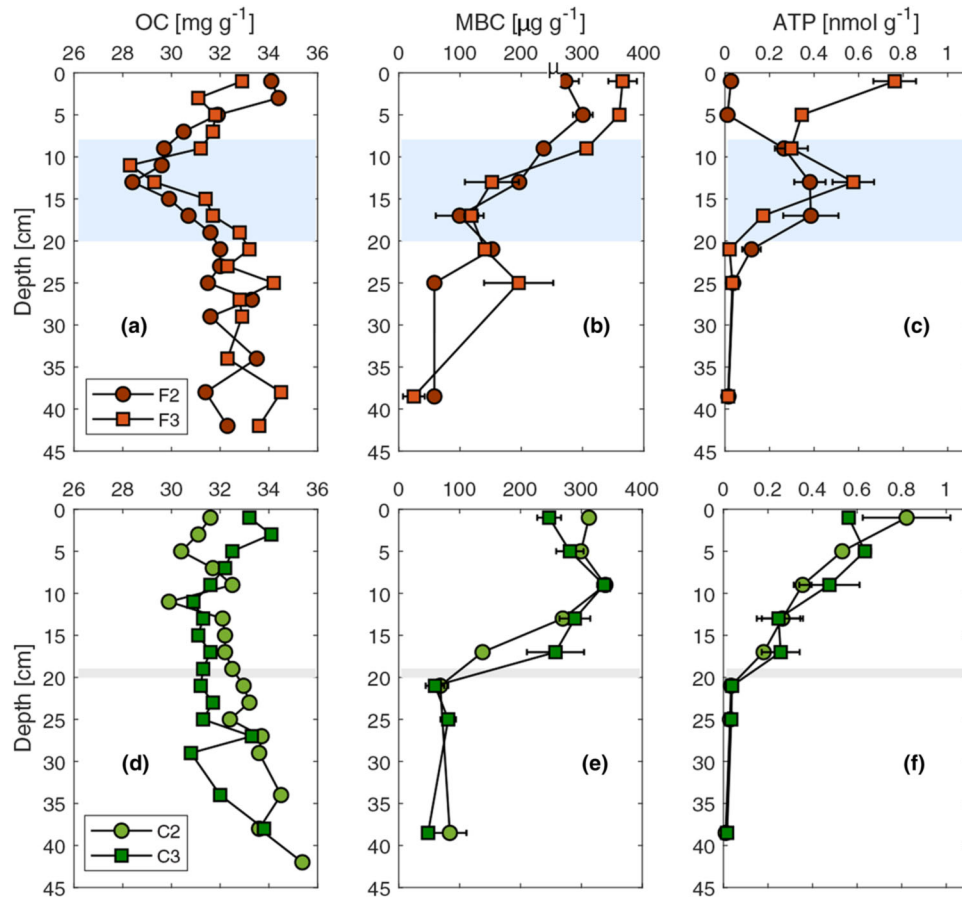


FIGURE 3 Depth profiles of (a, d) organic C (OC), (b, e) microbial biomass C (MBC), and soil (c, f) adenosine triphosphate (ATP) at the end of the incubation ($t = 329$ d). Top-row panels correspond to the fluctuating water table replicates, and bottom-row panels correspond to those of the static water table treatments. Blue rectangles denote the fluctuation zone interval (8–20 cm) in the fluctuating treatment columns, and gray intervals denote the static water level in columns C2 and C3. Prior to packing, the OC content of the homogenized artificial soil mixture was $35 \pm 3 \text{ mg g}^{-1}$

fluxes were computed based on the average concentration of DOC and DIC measured in fluctuating-column outflow samples during each drainage period and the corresponding total discharged volume (on average, 110 ml per drainage period). Both the DOC and DIC drainage fluxes were two orders of magnitude lower, each accounting for only 2% of the OC loss. The results thus imply that most OC was removed from the soil system via the efflux of CO_2 , whereas leaching of DIC and DOC were minor C sinks. Nonetheless, $\sim 24\%$ of the OC loss was not accounted for.

In addition to CO_2 , anaerobic degradation of OC can generate CH_4 . The measured CH_4 emissions, however, were very low, with values, after the initial 100 d of incubation, never exceeding $0.4 \mu\text{mol m}^{-2} \text{ s}^{-1}$, despite the water-logged anoxic conditions during the imbibition periods (weekly CH_4 flux measurements are presented in the supporting information, Supplemental Figure S6). Integrated over the entire time of the experiment, the efflux of CH_4 only represented 1.4% ($0.08 \pm 0.03 \text{ g C}$) of the OC loss (Figure 3b). Note that the weekly sampling schedule likely yields an underestimation of

total CH_4 emissions due to missed pulses. The suppression of CH_4 emissions during the imbibition periods was probably due, at least in part, to anaerobic respiration coupled to the reduction of inorganic and organic terminal electron acceptors. Dissimilatory Fe(III) and SO_4^{2-} reduction are possible respiration pathways, given the presence of goethite in the artificial soil mixture and the detection of measurable pore water SO_4^{2-} levels in the oxic and fluctuation zones (Supplemental Figure S2). Furthermore, natural organic matter may possess significant electron accepting capacity and support anaerobic production of CO_2 without concomitant production of CH_4 (Aeschbacher, Vergari, Schwarzenbach, & Sander, 2011; Gao, Sander, Agethen, & Knorr, 2019; Keller & Takagi, 2013), whereas the high relative abundance of CH_4 -oxidizing organisms (i.e., *Crenothrix* spp.) at the oxic–anoxic interface likely also limited CH_4 efflux (see Section 3.5).

Further work will be needed to identify and quantify all the various biotic and abiotic processes that control the fate of OC and the emissions of CO_2 under dynamic drainage and imbibition. These include the adsorption of DOC (Kothawala,

TABLE 1 Sample diversity in the 0- to 8-cm, 8- to 20-cm, and >20-cm depth intervals, after 99 and 329 d of incubation. Under a fluctuation water table, these depth intervals correspond to the oxic, fluctuation, and anoxic zones (see Section 3.2), respectively. In the static water columns, the depth of the water table is held constant at 20 cm below the soil surface. Error margins indicate the SD based on all samples from the corresponding depth interval (on average, 15 samples per depth). A two-sample *t* test was used to compare the average operational taxonomic unit (OTU) abundance between constant and fluctuating columns at the same depth interval

Depth cm	Observed OTUs after 99 d		Observed OTUs after 329 d	
	Static	Fluctuating	Static	Fluctuating
0–8	949.0 ± 48.8	994.3 ± 73.5	841.9 ± 74.9	864.6 ± 50.7
8–20	794.1 ± 173.9	930.1 ± 117.1	777.2 ± 79.3*	863.6 ± 100.4*
>20	693.7 ± 50.5	696.6 ± 41.6	667.8 ± 60.4	692.4 ± 45.7

*Significant at the .05 probability level.

Moore, & Hendershot, 2008), as well as the formation of carbonate mineral phases at the alkaline pore water pH values measured (Figure 1) and with Ca^{2+} and Mg^{2+} cations present in the artificial groundwater solution or Fe^{2+} produced by the dissimilatory reduction of goethite in the artificial soil matrix coupled with OC oxidation (Fredrickson et al., 1998). In addition, the closed chamber CO_2 flux calculations may underestimate the actual fluxes. Rayment (2000) found that closed chamber flux measurements yield an underestimation of 10% because the volume of air-filled pore space is not accounted for in the total volume for the flux calculation. Nevertheless, the available data imply that the observed OC loss during the experiments was mainly the result of microbially mediated degradation of the forest soil humus.

3.5 | Microbial community: Composition

The number of OTUs measured after 99 d and at the end of the experiment on dynamic and static water table columns are summarized in Table 1. The actual OTUs are shown in Supplemental Figures S7 and S8, for Days 99 and 329, respectively. The lowest numbers of OTUs were found in the deeper part of the columns, and the highest were found in the upper part. With the exception of the deepest samples collected after 99 d, the OTU counts were systematically higher in the dynamic compared with the static water table regime. The 8- to 20-cm depth interval exhibited the largest differences in OTU counts between the fluctuating and static water table regimes. In the fluctuating water table columns, the numbers of OTUs recovered from the fluctuation zone after 329 d were similar to those in the oxic zone, but significantly larger than in the anoxic zone. Thus, judging from the OTU counts, the fluctuating water table yielded a relatively higher microbial diversity than the static water table, particularly in the 8- to 20-cm depth interval (Table 1).

The 16S rRNA gene sequencing of 113 samples generated 2,652,681 assembled paired-end reads. After 99 and

329 d, the largest differences in microbial community composition were observed between the uppermost and deepest sections of the soil columns, under both fluctuating and static water table (Supplemental Figures S7 and S8). The differences between depth intervals were, in fact, more pronounced than between the two water table regimes, with the same taxa dominating in the same depth intervals. In both water table regimes, the most abundant gene sequences in the 0- to 8-cm soil depth were affiliated with Sinobacteraceae, Hyphomicrobiaceae, and Cytophagaceae, whereas OTUs affiliated with Crenotrichaceae (*Crenothrix* spp.) and Hyphomicrobiaceae (*Devosia* spp.) were most abundant in the 8- to 20-cm depth interval. Known aerobic organisms of *Devosia* spp. and Cytophagaceae were detected in the columns from 0 to ~16 cm before decreasing in abundance at greater depths. *Crenothrix* spp., which are known CH_4 -oxidizing organisms, were most abundant between 16- and 20-cm depths in all the columns. In the static water table columns, up to 16% of reads were affiliated with *Crenothrix* spp., and up to 18% were affiliated in the fluctuating water table columns. These high *Crenothrix* OTU counts may help explain the low CH_4 emissions measured during the experiment. At depths below 20 cm, OTUs affiliated with Bacteroidales, Clostridia, and Ignavibacteriales dominated in all columns at both time points (99 and 329 d).

In a previous experiment using the same column design, via denaturing gradient gel electrophoresis (DGGE), Rezanezhad et al. (2014) reported a lack of a pronounced differentiation in the microbial community structure between static and fluctuating water table conditions. We expected that the sequencing method used in the present study would be better suited to shed light on microbial community differences in response to a dynamic moisture regime. The microbial community in the fluctuation zone exhibited a higher OTU than its static counterpart (Table 1), indicating a slightly higher diversity of the microbial community present. However, the 16S rRNA gene analysis showed that, in corresponding depth intervals, the same major taxa dominated under both water table regimes.

This indicates that although the moisture fluctuations may have created additional niches supporting a higher community diversity, those differences do not seem to strongly affect overall microbial community structure.

By contrast, some earlier research with batch incubations found that shifts in soil aeration resulted in changes in microbial community diversity, composition, and functionality (Pett-Ridge & Firestone, 2005; Pícek, Šimek, & Šantrůčková, 2000), linked closely to redox-dependent N cycling (Pett-Ridge, Petersen, Nuccio, & Firestone, 2013; Randle-Boggis, Ashton, & Helgason, 2018). The latter was likely much less important in our experiment, because of the lack of N in the artificial groundwater and the high C/N ratio of the humus.

The presence of expandable clay and 10% humus yielded an artificial soil with a high water-retention capacity. Visual observation showed that during the entire drainage periods, the soil retained a wet aspect. Thus, even in the upper part of the soil, the microbial community was never exposed to complete desiccation, which in turn may have enabled the persistence of anaerobic microsites (Keiluweit, Wanzek, Kleber, Nico, & Fendorf, 2017; Sexstone, Revsbech, Parkin, & Tiedje, 1985). Furthermore, the initial microbial community was enriched from forest humus collected directly from a riparian zone and was likely already well adapted to variable redox conditions (Evans & Wallenstein, 2014). We therefore propose that the high OTUs in the fluctuation zone reflect the combination of a finite water retention, the persistence of local anoxic microsites during the periods of drainage, and the periodic ingress of O₂. How these conditions affect the activity of the microbial community is assessed in the section below.

3.6 | Microbial community: Biomass and activity

The turnover of MBC occurs over months and can be stabilized over significantly longer time scales (Miltner, Bombach, Schmidt-Brücken, & Kästner, 2012), whereas ATP is far less stable, providing a measure of metabolic activity on a timescale of days (Blagodatskaya & Kuzyakov, 2013). Thus, ATP provides microbial community activity information over a short period of time prior to sampling, whereas microbial biomass integrates longer term information and includes both active and dormant biota (Mellage et al., 2015; Stolpovsky, Fetzer, Van Cappellen, & Thullner, 2016).

The MBC concentrations were highest at the top of the columns and lowest in the bottom parts of both hydraulic regimes (Figures 3b and 4e). The concentrations in the aerobic zones of the columns fall toward the lower end of the range of previously reported MBC in soils with similar OC content (Blume et al., 2002). In the anaerobic zones, energetic limitation of microbial growth and activity in the absence of O₂ results in lower biomass C concentrations

(Inubushi, Brookes, and Jenkinson, 1991). In the static water table columns, biomass was relatively constant above the water table (~300 µg MBC g⁻¹ soil) and dropped abruptly to <100 µg MBC g⁻¹ soil below 20 cm (Figure 3e). In the fluctuating water table column, the biomass decreased gradually between 8 and 20 cm bss (Figure 3b). Therefore, in contrast with what might be expected, the zone of highest OC depletion did not coincide with a larger microbial population. In fact, at the depth where the lowest OC was measured in columns F2 and F3 (Figure 3a), roughly 13 cm bss, the biomass C concentration was only one-third of that at the same depth in the static water table columns C2 and C3.

The ATP concentrations in columns C2 and C3 gradually decreased with depth reaching levels near the limit of quantification below the water table (Figure 3f). The depth distributions of ATP under the fluctuating water table regime were markedly different (Figure 3c). In both columns F2 and F3, a peak in ATP was measured within the 8- to 20-cm fluctuation zone—that is, the depth interval with relatively low microbial biomass (Figure 4a) but the highest OC depletion (Figure 3a). Above 8 cm, columns F2 and F3 exhibited quite different ATP concentrations, with low values in F2 and relatively high values in F3. The reason for this difference is unknown. At depths >20 cm, the ATP concentrations in F2 and F3 dropped to levels comparable with those observed below 20 cm in the static water table columns. The ATP concentrations of the oxic portions of columns F3, C2, and C3 were at the lower end of the range reported for aerobic soils (Lin & Brookes, 1996; Qiu, Chen, Luo, Xu, & Brookes, 2016; Redmile-Gordon et al., 2011).

The ATP concentrations in Figures 4c and 4f are expressed per unit mass of soil. Alternatively, the ATP concentrations can be normalized to the MBC (ATP/MBC), as shown in Figure 5 (Panels a and c). The latter normalization yields biomass-specific activities with a peak value of 3.9 µmol ATP g⁻¹ MBC in the fluctuation zone of the dynamic water table columns (Figure 5a). By contrast, ATP/MBC values in the static hydraulic treatment were highest near the surface (Figure 5c, ~2.6 µmol ATP g⁻¹ MBC) and decreased steadily with depth. Within the 8- to 20-cm interval of the stable water table columns, ATP/MBC values were three times lower than in the same depth interval of the fluctuating water table columns. Together with the similar microbial community compositions across both water table regimes (Section 3.5), these results confirm the findings of Rezanezhad et al. (2014), who concluded that the preferential OC depletion under fluctuating water table conditions “primarily reflect differences in the activity of various components of the microbial community rather than major changes in community composition.”

The ATP maximum in the 8- to 20-cm zone of the fluctuating water table columns observed at the end of the experiment had not yet developed after 99 d, at which point the ATP profiles in the stable and fluctuating water table columns

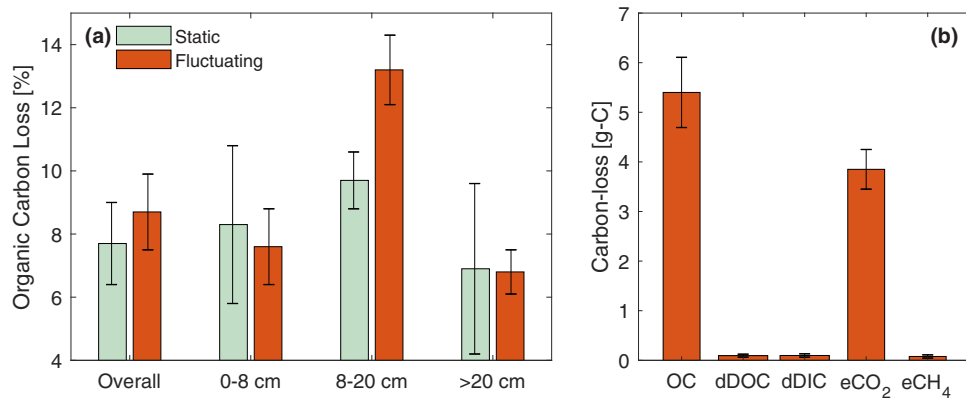


FIGURE 4 (a) Proportion of organic C (OC) loss in different depth intervals. The proportions are computed by subtracting the depth-dependent OC concentrations measured at the end of the incubation ($t = 329$ d) from the initial concentration in the homogenized artificial soil. Green bars are for the static water table treatment, and orange bars for the fluctuating water table treatment. Note that the 8- to 20-cm depth interval corresponds to the fluctuation zone in the fluctuating water table treatment. In the static water table columns, the water table is positioned at 20 cm below the soil surface. In both hydraulic treatments, the shallower and deeper intervals remained primarily aerobic and anaerobic, respectively. (b) The integrated OC loss, over the entire depth profile of fluctuating column F2, is compared with the outflow losses of C as dissolved organic C (DOC) and dissolved inorganic C (DIC) during drainage periods (dDOC, and dDIC, respectively), and the integrated CO₂ efflux (eCO₂) and CH₄ efflux (eCH₄) from the start to the end of the incubation experiment

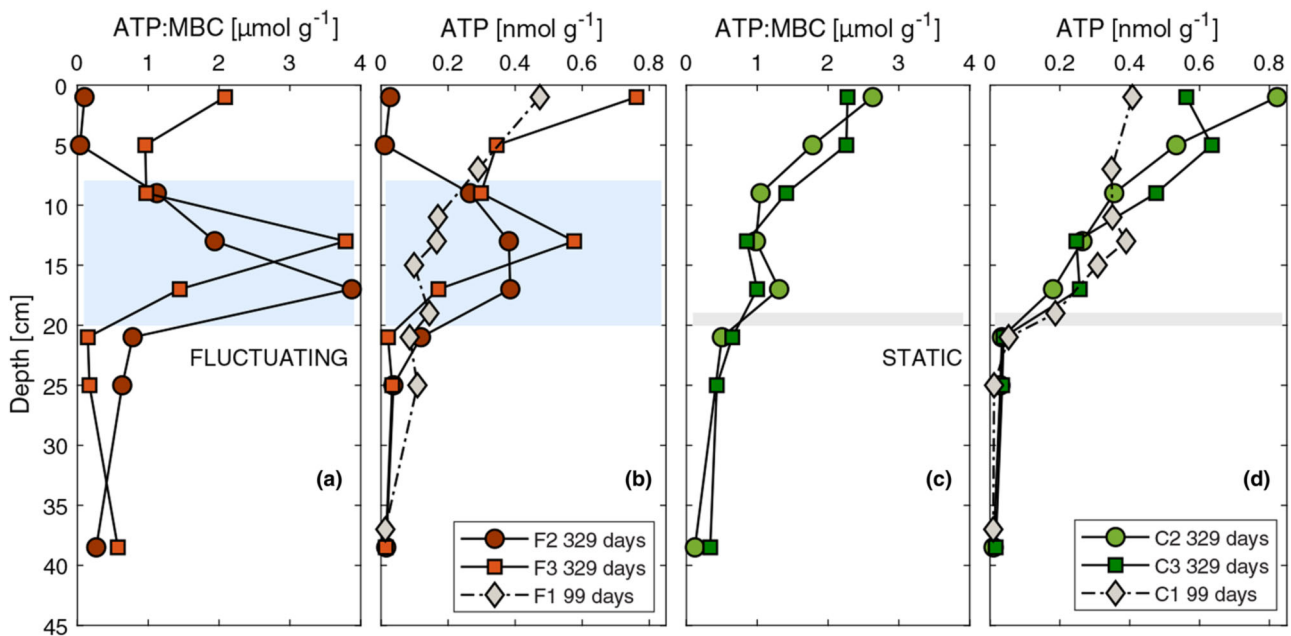


FIGURE 5 Depth-dependent adenosine triphosphate (ATP) concentrations, normalized to the concentration of microbial biomass C (MBC), for both the (a) fluctuating and (c) static treatment columns, after 329 d of incubation. Blue rectangles denote the fluctuation zone interval (8–20 cm) in the fluctuating treatment columns, and gray lines denote the static water level in columns C2 and C3. The ATP concentration depth distributions (as shown in Figure 3) are presented alongside in Panels b and d, with the additional inclusion of ATP depth profiles measured at 99 d (gray diamonds in Panels b and d)

were rather similar (Figures 5b and 5d). This suggests that during the first 99 d of incubation, the microbial populations were still adapting to the prevalent redox conditions, consistent with the OTU profiles at Day 99 that already showed

a differentiation in community composition between the top and bottom of the soil cores (Supplemental Figure S6). Overall, the microbial community structure and activity in our experimental soil columns responded on timescales that

are in line with previous studies that report soil microbial community development timescales on the order of 3–12 mo (Babin et al., 2013; Ding et al., 2013).

The enhanced OC turnover in the fluctuation zone of the dynamic water table columns was likely carried out by active cells that remained in a high-energy state in order to continuously adjust to changing O_2 availability and soil moisture, rather than relying on the reactivation of dormant cells (De Nobili, Contin, Mondini, & Brookes, 2001). Sardinha, Müller, Schmeisky, and Joergensen (2003) argue that environments inhabited by less “specialized” microbial communities result in more competition for resources between microbial species. Cells in a metabolically diverse community will therefore maintain a higher ATP to microbial biomass ratio as a survival strategy (De Nobili et al., 2001; Pfeiffer, Schuster, & Bonhoeffer, 2001). High levels of ATP production, however, are energy expensive and may translate into less growth (Fontaine, Mariotti, & Abbadie, 2003) while still requiring OC oxidation to meet maintenance requirements (Kleerebezem & Van Loosdrecht, 2010). The ATP/MBC profiles measured in our study similarly suggest that increased OC degradation under the dynamic redox conditions of the fluctuating water table soil columns was due to a more active, not a larger, microbial community.

4 | SUMMARY AND CONCLUSIONS

Water table fluctuations create spatially and temporally variable conditions in the soil environment. To identify potential impacts of these variable conditions on soil C dynamics, as well as the structure, abundance, and activity of the soil microbial population, we performed an 11-mo-long experiment on columns filled with an artificial soil matrix and inoculated with a microbial community from a riparian soil of a cold temperate deciduous forest. In one set of columns the water table remained at a fixed depth; in the other, drainage and imbibition cycles were imposed. Within the first 99 d, differences in the microbial community composition developed between the top and bottom portions of the columns, but little differentiation was observed between the static vs. fluctuating water table regimes. By the end of the experiment (329 d), however, taxonomic differences in the mid-column depth intervals (8–20 cm) had appeared between the two hydraulic regimes.

Under the fluctuating water table regime, the 8- to 20-cm interval (the fluctuation zone) experienced large oscillations in redox potential, pore water concentrations of O_2 , redox active constituents (Fe^{2+} , SO_4^{2-}), and DOC. The efflux of CO_2 further showed large variations in response to the water table fluctuations. At the end of the experiment, the fluctuation zone exhibited a distinct depletion of OC, compared with the upper (oxic zone) and lower (anoxic zone) soil layers. The water table fluctuations also yielded a somewhat

higher microbial diversity in the 8- to 20-cm interval, although under both hydraulic regimes the same taxa dominated at mid-depths.

The mid-depth OC depletion in the fluctuating water table columns did not coincide with higher MBC concentrations, but rather with peak values of the ATP/MBC ratios that were two to three times higher than in the same 8- to 20-cm depth interval of the static water table columns. These findings therefore imply that the enhanced OC degradation associated with the highly variable redox conditions in the fluctuation zone was driven by a metabolically more active soil microbial population, not a compositionally distinct or more abundant microbial population. Further work will be needed to comprehensively delineate the biogeochemical mechanisms and ecological interactions that are responsible for the higher soil OC turnover under fluctuating water table conditions, and to determine their overall impact on C cycling and fluxes in real-world soil systems.

CONFLICT OF INTEREST

The authors declare no conflict of interest.

ACKNOWLEDGMENTS

The work of G.J. Pronk was funded by a Research Fellowship of the German Research Foundation (DFG, PR1550/1-1). Additional support was received from the Canada Excellence Research Chair (CERC) program in Ecohydrology, the Waterloo-Technion University Cooperation Programme, Natural Sciences and Engineering Research Council (NSERC) Strategic Partnership Grant (STPGP494652-16), the Global Water Futures (GWF) funded under the Canada First Excellence Research Fund (CFREF), and the Training Toward Environmentally Responsible Resource Extraction (TERRE)-Collaborative Research and Training Experience program and courses. The authors thank Marianne Vandergriendt, Linden Fairbairn, and Riley Mills for their assistance with laboratory analyses. We also thank the *rare* Charitable Research Reserve (Cambridge, ON, Canada) for access to the field site where some samples were collected.

ORCID

Adrian Mellage  <https://orcid.org/0000-0003-2708-4518>

Josh D. Neufeld  <https://orcid.org/0000-0002-8722-8571>

REFERENCES

- Aeschbacher, M., Vergari, D., Schwarzenbach, R. P., & Sander, M. (2011). Electrochemical analysis of proton and electron transfer equilibria of the reducible moieties in humic acids. *Environmental Science & Technology*, 45, 8385–8394. <https://doi.org/10.1021/es201981g>.
- Anderson, M. J. (2001). A new method for non-parametric multivariate analysis of variance. *Austral Ecology*, 26, 32–46. <https://doi.org/10.1111/j.1442-9993.2001.01070.pp.x>

- Apostol, I., Miller, K. J., Ratto, J., & Kelner, D. N. (2009). Comparison of different approaches for evaluation of the detection and quantitation limits of a purity method: A case study using a capillary isoelectrofocusing method for a monoclonal antibody. *Analytical Biochemistry*, 385, 101–106. <https://doi.org/10.1016/j.ab.2008.09.053>
- Babin, D., Ding, G.-C., Pronk, G. J., Heister, K., Kögel-Knabner, I., & Smalla, K. (2013). Metal oxides, clay minerals and charcoal determine the composition of microbial communities in matured artificial soils and their response to phenanthrene. *FEMS Microbiology Ecology*, 86, 3–14. <https://doi.org/10.1111/1574-6941.12058>
- Badocco, D., Mondin, A., & Pastore, P. (2012). Determination of thermodynamic parameters from light intensity signals obtained from oxygen optical sensors. *Sensors and Actuators B: Chemical*, 163, 165–170. <https://doi.org/10.1016/j.snb.2012.01.030>
- Bartram, A. K., Lynch, M. D., Stearns, J. C., Moreno-Hagelsieb, G., & Neufeld, J. D. (2011). Generation of multimillion-sequence 16S rRNA gene libraries from complex microbial communities by assembling paired-end Illumina reads. *Applied and Environmental Microbiology*, 77, 3846–3852. <https://doi.org/10.1128/AEM.02772-10>
- Berkowitz, B., Silliman, S. E., & Dunn, A. M. (2004). Impact of the capillary fringe on local flow, chemical migration, and microbiology. *Vadose Zone Journal*, 3, 534–548. <https://doi.org/10.2136/vzj2004.0534>
- Blagodatskaya, E., & Kuzyakov, Y. (2013). Active microorganisms in soil: Critical review of estimation criteria and approaches. *Soil Biology & Biochemistry*, 67, 192–211. <https://doi.org/10.1016/j.soilbio.2013.08.024>
- Blume, E., Bischoff, M., Reichert, J., Moorman, T., Konopka, A., & Turco, R. J. A. S.E. (2002). Surface and subsurface microbial biomass, community structure and metabolic activity as a function of soil depth and season. *Applied Soil Ecology*, 20, 171–181. [https://doi.org/10.1016/S0929-1393\(02\)00025-2](https://doi.org/10.1016/S0929-1393(02)00025-2)
- Bray, J. R., & Curtis, J. T. (1957). An ordination of the upland forest communities of southern Wisconsin. *Ecological Monographs*, 27, 325–349. <https://doi.org/10.2307/1942268>
- Caporaso, J. G., Kuczynski, J., Stombaugh, J., Bittinger, K., Bushman, F. D., Costello, E. K., ... Knight, R. (2010). QIIME allows analysis of high-throughput community sequencing data. *Nature Methods*, 7, 335–336. <https://doi.org/10.1038/nmeth.f.303>
- Cleveland, C. C., Wieder, W. R., Reed, S. C., & Townsend, A. R. (2010). Experimental drought in a tropical rain forest increases soil carbon dioxide losses to the atmosphere. *Ecology*, 91, 2313–2323. <https://doi.org/10.1890/09-1582.1>
- Dassonville, F., & Renault, P. (2002). Interactions between microbial processes and geochemical transformations under anaerobic conditions: A review. *Agronomie*, 22, 51–68. <https://doi.org/10.1051/agro:2001001>
- Davidson, E., Savage, K., Verchot, L., & Navarro, R. (2002). Minimizing artifacts and biases in chamber-based measurements of soil respiration. *Agricultural and Forest Meteorology*, 113, 21–37. [https://doi.org/10.1016/S0168-1923\(02\)00100-4](https://doi.org/10.1016/S0168-1923(02)00100-4)
- De Nobili, M., Contin, M., Mondini, C., & Brookes, P. (2001). Soil microbial biomass is triggered into activity by trace amounts of substrate. *Soil Biology & Biochemistry*, 33, 1163–1170.
- DeAngelis, K. M., Silver, W. L., Thompson, A. W., & Firestone, M. K. (2010). Microbial communities acclimate to recurring changes in soil redox potential status. *Environmental Microbiology*, 12, 3137–3149. <https://doi.org/10.1111/j.1462-2920.2010.02286.x>
- Ding, G.-C., Pronk, G. J., Babin, D., Heuer, H., Heister, K., Kögel-Knabner, I., ... Smalla, K. (2013). Mineral composition and charcoal determine the bacterial community structure in artificial soils. *FEMS Microbiology Ecology*, 86, 15–25. <https://doi.org/10.1111/1574-6941.12070>
- Dufrêne, M., & Legendre, P. (1997). Species assemblages and indicator species: The need for a flexible asymmetrical approach. *Ecological Monographs*, 67, 345–366. [https://doi.org/10.1890/0012-9615\(1997\)067\[0345:SAAI\]2.0.CO;2](https://doi.org/10.1890/0012-9615(1997)067[0345:SAAI]2.0.CO;2)
- Ebrahimi, A., & Or, D. (2018). Dynamics of soil biogeochemical gas emissions shaped by remolded aggregate sizes and carbon configurations under hydration cycles. *Global Change Biology*, 24, E378–E392. <https://doi.org/10.1111/gcb.13938>
- Edgar, R. C. (2013). UPARSE: Highly accurate OTU sequences from microbial amplicon reads. *Nature Methods*, 10, 996–998. <https://doi.org/10.1038/nmeth.2604>
- Epron, D., Farque, L., Lucot, É., & Badot, P.-M. (1999). Soil CO₂ efflux in a beech forest: Dependence on soil temperature and soil water content. *Annals of Forest Science*, 56, 221–226. <https://doi.org/10.1051/forest:19990304>
- Evans, S. E., & Wallenstein, M. D. (2014). Climate change alters ecological strategies of soil bacteria. *Ecology Letters*, 17, 155–164. <https://doi.org/10.1111/ele.12206>
- Fontaine, S., Mariotti, A., & Abbadie, L. (2003). The priming effect of organic matter: A question of microbial competition? *Soil Biology & Biochemistry*, 35, 837–843. [https://doi.org/10.1016/S0038-0717\(03\)00123-8](https://doi.org/10.1016/S0038-0717(03)00123-8)
- Fredrickson, J. K., Zachara, J. M., Kennedy, D. W., Dong, H., Onstott, T. C., Hinman, N. W., & Li, S. (1998). Biogenic iron mineralization accompanying the dissimilatory reduction of hydrous ferric oxide by a groundwater bacterium. *Geochimica et Cosmochimica Acta*, 62, 3239–3257. [https://doi.org/10.1016/S0016-7037\(98\)00243-9](https://doi.org/10.1016/S0016-7037(98)00243-9)
- Gao, C., Sander, M., Agethen, S., & Knorr, K.-H. (2019). Electron accepting capacity of dissolved and particulate organic matter control CO₂ and CH₄ formation in peat soils. *Geochimica et Cosmochimica Acta*, 245, 266–277. <https://doi.org/10.1016/j.gca.2018.11.004>
- Gower, J. C. (1966). Some distance properties of latent root and vector methods used in multivariate analysis. *Biometrika*, 53, 325–338. <https://doi.org/10.1093/biomet/53.3-4.325>
- Haberer, C. M., Rolle, M., Cirpka, O. A., & Grathwohl, P. (2012). Oxygen transfer in a fluctuating capillary fringe. *Vadose Zone Journal*, 11(3). <https://doi.org/10.2136/vzj2011.0056>
- Hanson, P., Wullschlegel, S., Bohlman, S., & Todd, D. (1993). Seasonal and topographic patterns of forest floor CO₂ efflux from an upland oak forest. *Tree Physiology*, 13, 1–15. <https://doi.org/10.1093/treephys/13.1.1>
- Hefting, M., Clément, J.-C., Dowrick, D., Cosandey, A.-C., Bernal, S., Cimpian, C., ... Pinay, G. (2004). Water table elevation controls on soil nitrogen cycling in riparian wetlands along a European climatic gradient. *Biogeochemistry*, 67, 113–134. <https://doi.org/10.1023/B: BIOG.0000015320.69868.33>
- Huang, W. J., & Hall, S. J. (2017). Elevated moisture stimulates carbon loss from mineral soils by releasing protected organic matter. *Nature Communications*, 8. <https://doi.org/10.1038/s41467-017-01998-z>
- Huang, W. J., Hammel, K. E., Hao, J. L., Thompson, A., Timokhin, V. I., & Hall, S. J. (2019). Enrichment of lignin-derived carbon in mineral-associated soil organic matter. *Environmental Science & Technology*, 53, 7522–7531. <https://doi.org/10.1021/acs.est.9b01834>

- Inubushi, K., Brookes, P. C., & Jenkinson, D. S. (1991). Soil microbial biomass C, N and ninhydrin-N in aerobic and anaerobic soils measured by the fumigation-extraction method. *Soil Biology & Biochemistry*, 23, 737–741. [https://doi.org/10.1016/0038-0717\(91\)90143-8](https://doi.org/10.1016/0038-0717(91)90143-8)
- Jenkinson, D., & Oades, J. (1979). A method for measuring adenosine triphosphate in soil. *Soil Biology & Biochemistry*, 11, 193–199. [https://doi.org/10.1016/0038-0717\(79\)90100-7](https://doi.org/10.1016/0038-0717(79)90100-7)
- Joergensen, R. G., & Mueller, T. (1996). The fumigation-extraction method to estimate soil microbial biomass: Calibration of the k(EN) value. *Soil Biology & Biochemistry*, 28, 33–37. [https://doi.org/10.1016/0038-0717\(95\)00101-8](https://doi.org/10.1016/0038-0717(95)00101-8)
- Jost, D., Winter, J., & Gallert, C. (2011). Water and oxygen dependence of *Pseudomonas putida* growing in silica sand capillary fringes. *Vadose Zone Journal*, 10, 532–540. <https://doi.org/10.2136/vzj2010.0092>
- Keiluweit, M., Nico, P. S., Kleber, M., & Fendorf, S. (2016). Are oxygen limitations under recognized regulators of organic carbon turnover in upland soils? *Biogeochemistry*, 127, 157–171. <https://doi.org/10.1007/s10533-015-0180-6>
- Keiluweit, M., Wanzek, T., Kleber, M., Nico, P., & Fendorf, S. (2017). Anaerobic microsites have an unaccounted role in soil carbon stabilization. *Nature Communications*, 8. <https://doi.org/10.1038/s41467-017-01406-6>
- Keller, J. K., & Takagi, K. K. (2013). Solid-phase organic matter reduction regulates anaerobic decomposition in bog soil. *Ecosphere*, 4(5). <https://doi.org/10.1890/es12-00382.1>
- Kleerebezem, R., & Van Loosdrecht, M. C. (2010). A generalized method for thermodynamic state analysis of environmental systems. *Critical Reviews in Environmental Science and Technology*, 40, 1–54. <https://doi.org/10.1080/10643380802000974>
- Klüpfel, L., Piepenbrock, A., Kappler, A., & Sander, M. (2014). Humic substances as fully regenerable electron acceptors in recurrently anoxic environments. *Nature Geoscience*, 7, 195–200. <https://doi.org/10.1038/ngeo2084>
- Kothawala, D. N., Moore, T. R., & Hendershot, W. H. (2008). Adsorption of dissolved organic carbon to mineral soils: A comparison of four isotherm approaches. *Geoderma*, 148, 43–50. <https://doi.org/10.1016/j.geoderma.2008.09.004>
- Larsen, M., Borisov, S. M., Grunwald, B., Klimant, I., & Glud, R. N. (2011). A simple and inexpensive high resolution color ratiometric planar optode imaging approach: Application to oxygen and pH sensing. *Limnology and Oceanography: Methods*, 9, 348–360. <https://doi.org/10.4319/lom.2011.9.348>
- Lin, Q., & Brookes, P. (1996). Comparison of methods to measure microbial biomass in unamended, ryegrass-amended and fumigated soils. *Soil Biology & Biochemistry*, 28, 933–939. [https://doi.org/10.1016/0038-0717\(96\)00058-2](https://doi.org/10.1016/0038-0717(96)00058-2)
- Lynch, M. D., Masella, A. P., Hall, M. W., Bartram, A. K., & Neufeld, J. D. (2013). AXIOME: Automated exploration of microbial diversity. *GigaScience*, 2(1). <https://doi.org/10.1186/2047-217X-2-3>
- Masella, A. P., Bartram, A. K., Truszkowski, J. M., Brown, D. G., & Neufeld, J. D. (2012). PANDAseq: Paired-end assembler for Illumina sequences. *BMC Bioinformatics*, 13. <https://doi.org/10.1186/1471-2105-13-31>
- McClain, M. E., Boyer, E. W., Dent, C. L., Gergel, S. E., Grimm, N. B., Groffman, P. M., ... Pinay, G. (2003). Biogeochemical hot spots and hot moments at the interface of terrestrial and aquatic ecosystems. *Ecosystems*, 6, 301–312. <https://doi.org/10.1007/s10021-003-0161-9>
- McDonald, D., Price, M. N., Goodrich, J., Nawrocki, E. P., DeSantis, T. Z., Probst, A., ... Hugenholtz, P. (2012). An improved GreenGenes taxonomy with explicit ranks for ecological and evolutionary analyses of bacteria and archaea. *ISME Journal*, 6, 610–618. <https://doi.org/10.1038/ismej.2011.139>
- Mellage, A., Eckert, D., Grösbacher, M., Inan, A. Z., Cirpka, O. A., & Griebler, C. (2015). Dynamics of suspended and attached aerobic toluene degraders in small-scale flow-through sediment systems under growth and starvation conditions. *Environmental Science & Technology*, 49, 7161–7169. <https://doi.org/10.1021/es5058538>
- Miltner, A., Bombach, P., Schmidt-Brücken, B., & Kästner, M. (2012). SOM genesis: Microbial biomass as a significant source. *Biogeochemistry*, 111, 41–55. <https://doi.org/10.1007/s10533-011-9658-z>
- Moyano, F. E., Manzoni, S., & Chenu, C. (2013). Responses of soil heterotrophic respiration to moisture availability: An exploration of processes and models. *Soil Biology & Biochemistry*, 59, 72–85. <https://doi.org/10.1016/j.soilbio.2013.01.002>
- Oertel, C., Matschullat, J., Zurba, K., Zimmermann, F., & Erasmí, S. (2016). Greenhouse gas emissions from soils: A review. *Geochemistry*, 76, 327–352. <https://doi.org/10.1016/j.jchemer.2016.04.002>
- Pett-Ridge, J., & Firestone, M. (2005). Redox fluctuation structures microbial communities in a wet tropical soil. *Applied and Environmental Microbiology*, 71, 6998–7007. <https://doi.org/10.1128/AEM.71.11.6998-7007.2005>
- Pett-Ridge, J., Petersen, D. G., Nuccio, E., & Firestone, M. K. (2013). Influence of oxic/anoxic fluctuations on ammonia oxidizers and nitrification potential in a wet tropical soil. *FEMS Microbiology Ecology*, 85, 179–194. <https://doi.org/10.1111/1574-6941.12111>
- Pett-Ridge, J., Silver, W. L., & Firestone, M. K. (2006). Redox fluctuations frame microbial community impacts on N-cycling rates in a humid tropical forest soil. *Biogeochemistry*, 81, 95–110. <https://doi.org/10.1007/s10533-006-9032-8>
- Pfeiffer, T., Schuster, S., & Bonhoeffer, S. (2001). Cooperation and competition in the evolution of ATP-producing pathways. *Science*, 292, 504–507. <https://doi.org/10.1126/science.1058079>
- Picek, T., Šimek, M., & Šantrůčková, H. (2000). Microbial responses to fluctuation of soil aeration status and redox conditions. *Biology and Fertility of Soils*, 31, 315–322. <https://doi.org/10.1007/s003740050662>
- Pronk, G. J., Heister, K., Ding, G.-C., Smalla, K., & Kögel-Knabner, I. (2012). Development of biogeochemical interfaces in an artificial soil incubation experiment; aggregation and formation of organo-mineral associations. *Geoderma*, 189, 585–594. <https://doi.org/10.1016/j.geoderma.2012.05.020>
- Pronk, G. J., Heister, K., Vogel, C., Babin, D., Bachmann, J., Ding, G.-C., ... Kögel-Knabner, I. (2017). Interaction of minerals, organic matter, and microorganisms during biogeochemical interface formation as shown by a series of artificial soil experiments. *Biology and Fertility of Soils*, 53, 9–22. <https://doi.org/10.1007/s00374-016-1161-1>
- Qiu, G., Chen, Y., Luo, Y., Xu, J., & Brookes, P. C. (2016). The microbial ATP concentration in aerobic and anaerobic Chinese soils. *Soil Biology & Biochemistry*, 92, 38–40. <https://doi.org/10.1016/j.soilbio.2015.09.009>
- Randle-Boggis, R. J., Ashton, P. D., & Helgason, T. (2018). Increasing flooding frequency alters soil microbial communities and functions under laboratory conditions. *MicrobiologyOpen*, 7(1). <https://doi.org/10.1002/mbo3.548>
- Rasband, W. S. (2015). *ImageJ*. Bethesda, MD: National Institutes of Health.

- Rayment, M. B. (2000). Closed chamber systems underestimate soil CO₂ efflux. *European Journal of Soil Science*, *51*, 107–110. <https://doi.org/10.1046/j.1365-2389.2000.00283.x>
- Redmile-Gordon, M., White, R., & Brookes, P. (2011). Evaluation of substitutes for paraquat in soil microbial ATP determinations using the trichloroacetic acid based reagent of Jenkinson and Oades (1979). *Soil Biology & Biochemistry*, *43*, 1098–1100. <https://doi.org/10.1016/j.soilbio.2011.01.007>
- Rezanezhad, F., Couture, R.-M., Kovac, R., O'Connell, D., & Van Cappellen, P. (2014). Water table fluctuations and soil biogeochemistry: An experimental approach using an automated soil column system. *Journal of Hydrology*, *509*, 245–256. <https://doi.org/10.1016/j.jhydrol.2013.11.036>
- Saiyouri, N., Hicher, P. Y., & Tessier, D. (2000). Microstructural approach and transfer water modelling in highly compacted unsaturated swelling clays. *Mechanics of Cohesive-frictional Materials*, *5*, 41–60. [https://doi.org/10.1002/\(SICI\)1099-1484\(200001\)5:1%3c41::AID-CFM75%3e3.0.CO;2-N](https://doi.org/10.1002/(SICI)1099-1484(200001)5:1%3c41::AID-CFM75%3e3.0.CO;2-N)
- Sardinha, M., Müller, T., Schmeisky, H., & Joergensen, R. G. (2003). Microbial performance in soils along a salinity gradient under acidic conditions. *Applied Soil Ecology*, *23*, 237–244. [https://doi.org/10.1016/S0929-1393\(03\)00027-1](https://doi.org/10.1016/S0929-1393(03)00027-1)
- Sexstone, A. J., Revsbech, N. P., Parkin, T. B., & Tiedje, J. M. (1985). Direct measurement of oxygen profiles and denitrification rates in soil aggregates. *Soil Science Society of America Journal*, *49*, 645–651. <https://doi.org/10.2136/sssaj1985.03615995004900030024x>
- Stegen, J. C., Fredrickson, J. K., Wilkins, M. J., Konopka, A. E., Nelson, W. C., Arntzen, E. V., ... Tfaily, M. (2016). Groundwater-surface water mixing shifts ecological assembly processes and stimulates organic carbon turnover. *Nature Communications*, *7*. <https://doi.org/10.1038/ncomms11237>
- Stolpovsky, K., Fetzer, I., Van Cappellen, P., & Thullner, M. (2016). Influence of dormancy on microbial competition under intermittent substrate supply: Insights from model simulations. *FEMS Microbiology Ecology*, *92*(6). <https://doi.org/10.1093/femsec/fiw071>
- Takahashi, S., Tomiata, J., Nishioka, K., Hisada, T., & Nishijima, M. (2014). Development of a prokaryotic universal primer for simultaneous analysis of bacteria and archaea using next-generation sequencing *PLOS ONE*, *9*(8). <https://doi.org/10.1371/journal.pone.0105592>
- Vance, E. D., Brookes, P. C., & Jenkinson, D. S. (1987). An extraction method for measuring soil microbial biomass C. *Soil Biology & Biochemistry*, *19*, 703–707. [https://doi.org/10.1016/0038-0717\(87\)90052-6](https://doi.org/10.1016/0038-0717(87)90052-6)
- Viollier, E., Inglett, P., Hunter, K., Roychoudhury, A., & Van Cappellen, P. (2000). The ferrozine method revisited: Fe (II)/Fe (III) determination in natural waters. *Applied Geochemistry*, *15*, 785–790. [https://doi.org/10.1016/S0883-2927\(99\)00097-9](https://doi.org/10.1016/S0883-2927(99)00097-9)
- Vogel, C., Babin, D., Pronk, G. J., Heister, K., Smalla, K., & Kögel-Knabner, I. (2014). Establishment of macro-aggregates and organic matter turnover by microbial communities in long-term incubated artificial soils. *Soil Biology & Biochemistry*, *79*, 57–67. <https://doi.org/10.1016/j.soilbio.2014.07.012>
- Vos, M., Wolf, A. B., Jennings, S. J., & Kowalchuk, G. A. (2013). Micro-scale determinants of bacterial diversity in soil. *FEMS Microbiology Reviews*, *37*, 936–954. <https://doi.org/10.1111/1574-6976.12023>
- Wang, C., Han, Y., Chen, J., Wang, X., Zhang, Q., & Bond-Lamberty, B. (2013). Seasonality of soil CO₂ efflux in a temperate forest: Biophysical effects of snowpack and spring freeze–thaw cycles. *Agricultural and Forest Meteorology*, *177*, 83–92. <https://doi.org/10.1016/j.agrformet.2013.04.008>
- Wang, J. H., Bogena, H. R., Vereecken, H., & Bruggemann, N. (2018). Characterizing redox potential effects on greenhouse gas emissions induced by water-level changes. *Vadose Zone Journal*, *17*(1). <https://doi.org/10.2136/vzj2017.08.0152>
- Wang, Q., Garrity, G. M., Tiedje, J. M., & Cole, J. R. (2007). Naive Bayesian classifier for rapid assignment of rRNA sequences into the new bacterial taxonomy. *Applied and Environmental Microbiology*, *73*, 5261–5267. <https://doi.org/10.1128/aem.00062-07>
- Xie, M., Agus, S. S., Schanz, T., & Kolditz, O. (2004). An upscaling method and a numerical analysis of swelling/shrinking processes in a compacted bentonite/sand mixture. *International Journal for Numerical and Analytical Methods in Geomechanics*, *28*, 1479–1502. <https://doi.org/10.1002/nag.396>
- Yu, K., Faulkner, S. P., & Baldwin, M. J. (2008). Effect of hydrological conditions on nitrous oxide, methane, and carbon dioxide dynamics in a bottomland hardwood forest and its implication for soil carbon sequestration. *Global Change Biology*, *14*, 798–812. <https://doi.org/10.1111/j.1365-2486.2008.01545.x>

SUPPORTING INFORMATION

Additional supporting information may be found online in the Supporting Information section at the end of the article.

How to cite this article: Pronk GJ, Mellage A, Milojevic T, et al. Carbon turnover and microbial activity in an artificial soil under imposed cyclic drainage and imbibition. *Vadose Zone J.* 2020;19:e20021 <https://doi.org/10.1002/vzj2.20021>